

# Orientation of smooth muscle cells with application in mechanical model of gastropod tissue

P. Kochová<sup>a,\*</sup>, R. Cimrman<sup>a</sup>, E. Rohan<sup>a</sup>

<sup>a</sup>Faculty of Applied Sciences, University of West Bohemia, Univerzitní 22, 306 14 Plzeň, Czech Republic

Received 31 August 2008; received in revised form 25 February 2009

---

## Abstract

In this paper, we determine the spatial orientation of smooth muscle cells of gastropod tissue. This together with volume fractions of smooth muscle cells and other tissue components obtained using stereological methods serves as input data for our mechanical model of gastropod tissue. The mechanical model is a composite model consisting of various components chosen to describe key features of the tissue like elasticity and viscoelasticity and preferential directions of muscle fibres. The elastic and viscoelastic constitutive parameters are identified by an automatic identification procedure based on nonlinear least squares. Numerical examples of the identification using real experimental data from uniaxial tension tests are shown.

© 2009 University of West Bohemia. All rights reserved.

*Keywords:* length density, composite model, smooth muscle tissue, spatial orientation, volume fraction

---

## 1. Introduction

The biological tissues and organs represent very complex structures [21]. They are composed from many types of cells (such as fibroblasts, muscle, fat, immune cells) and fibres (such as collagen and elastin). These structures are three-dimensional objects with random or preferential orientations in space. Mathematically, these structures are modelled as stationary fibre processes in space. In a case of stationarity, a basic characteristic of the fibre processes (cells, fibres) is the intensity, e.g. the mean fibre length per unit volume. The structures have also associated directions (of tangents or normals) and this leads to another important structural characterization by the rose of directions [22] which indicates, for example, that some directions of the fibres are preferred [10]. Concerning state of the art, there are few studies describing the two-dimensional orientation, e.g. smooth muscle cells within the wall of porcine abdominal aorta [23], but there is a lack of studies describing the three-dimensional orientation of fibres reconstructed from physical sections. In this context we stress out that much research has been done in the mathematical modeling of arterial walls using stable constitutive law formulations based on structural tensors, cf. [4] where the fibre dispersion is considered.

There are many studies describing computational models suitable for soft tissue modelling, but there is always a problem of matching the models with measurements. On the other hand, only a few studies combine the actual mechanical measurements of living tissues with spatial orientation of main tissue components. The notable exceptions are [4, 7] and [8], where a fibre-reinforced circular tube is described, composed of isotropic and transversely isotropic/orthotropic layers, used as a model of arterial wall.

---

\*Corresponding author. Tel.: +420 377 632 364, e-mail: kochovap@kme.zcu.cz.

This article extends our previous research devoted to mechanical and structural properties of smooth muscle of gastropods, cf. [11]. Its novelty lies in employing both the quantitative microscopy information on the spatial tissue structure and the mechanical measurements of macroscopic specimens to identify the parameters of complex mathematical model of the tissue. It is structured as follows: after providing a necessary theoretical background in Section 2, the volume fractions of main tissue components (smooth muscle cells, extracellular matrix) and the preferential directions of smooth muscle cells of gastropod tissue are determined in Section 3.1. These data are then included in the computational model and the constitutive parameters of the model are identified using stress-strain curves obtained from measurements on the living gastropod tissue in Section 3.2.

## **2. Material and Methods**

### *2.1. Material*

A sample of the gastropod tissue was excised from the sole of gastropod body. The sample used for mechanical measurements was processed to the size suitable for measurement devices. Tissue samples located near those used for the mechanical measurements underwent histological analysis. The samples were prepared by standard histological methods, as described in Section 2.3.

The tissue of gastropod *Arion sp.* was chosen to be a subject of the mechanical and stereological research because of its very convenient properties. The tissue has similar constituents as the mammalian smooth muscle tissue: smooth muscle cells (SMC), connective tissue composed mostly from collagen fibrils, fibroblast, neural, immune and fat cells. Moreover, gastropods belong to the group of ectothermic organisms. This phylogenetic affinity guarantees a small standard metabolic rate. A sample cut off from the gastropod body stays alive for several hours, allowing thus to measure the living muscle tissue at room temperature without using any preservative agents.

The individual SMC of the sole of gastropod are spindle shaped and are arranged into a three-dimensional network, similar to the vascular smooth muscle cells in rabbit mesenteric arterioles [16]. The collagen fibres surround the SMC and create a three-dimensional network similarly to blood vessels [3].

### *2.2. Mechanical Testing*

The measurement protocol is described in detail in [12] and [13]. A sample of the tissue cut off the sole of gastropod foot was subjected to a uniaxial tension test with the loading rate 20 mN/minute and to a creep test with a constant stress of 10.6 kPa. The loading was aligned to the main axis of the gastropod body. The resulting stress-strain curves were used to determine the parameters of the mechanical model described in Section 2.6.

### *2.3. Histology*

A piece of the tissue cut off the sole of gastropod foot was removed for histological processing [1]. The sample was perfused with 10% buffered formalin and embedded in paraffin.

Each brick of paraffine with the tissue sample was cut using the microtome Leica RM 2135 (Leica Microsystems GmbH, Germany) into 72 serial sections (thickness of 5  $\mu\text{m}$ ). To obtain the vertical uniform random (VUR) sections, cf. [9], the following procedure was used. Firstly, the plane defined by the gastropod sole was selected as an arbitrary horizontal reference plane.

The brick with the sample was then rotated around vertical axis perpendicular to the reference plane and finally, cut into 72 parallel sections.

The VUR sections were placed on glass slides, stained with Mallory's trichrome and hematoxylin-eosin [24], and covered by cover slips.

#### *2.4. Quantitative Microscopy*

The microscope Olympus BX51, with objectives UPlanSApo 2×/0.060 and 20×/0.750 connected with the digital camera Camedia C5060WZ directed by the software QuickPhoto Micro 2.0 (Olympus C&S, Prague, Czech Republic) were used for observation and recording, see fig. 1. The resolution of pictures used for the stereological analysis was  $1\,280 \times 960$  pixels.

The software Ellipse3D (ViDiTo company, Košice, Slovak Republic) was used for the stereological measurements. This software implements the most used stereological methods, for example the Cavalieri method (module PointGrid), the Buffon's needle method (module LineSystem), the physical disector method (module Disector) and the rose of directions (module Orientation3D) for estimating the numerical, length and surface densities, the mean volume and spatial orientation of smooth muscle cells, described in detail in [6, 9, 15].

#### *2.5. The Smooth Muscle and Connective Tissue of Gastropods*

The structure of smooth muscle and connective tissue of gastropods is shown in fig. 1: Fig. 1 (left) shows the section perpendicular to the main axis of the gastropod body. Mucus-containing cells in the epithelium and subepithelial tissue in ventral integument are significantly visible on the top of tissue. Fig. 1 (right) shows the deeper layer of gastropod foot. Subepithelial collagenous connective tissue (blue/lighter) with three-dimensional meshwork of smooth muscle cell bundles (reddish/darker). The optical empty spaces (white) are haemocoelic sinuses filled with body liquid under physiological conditions.

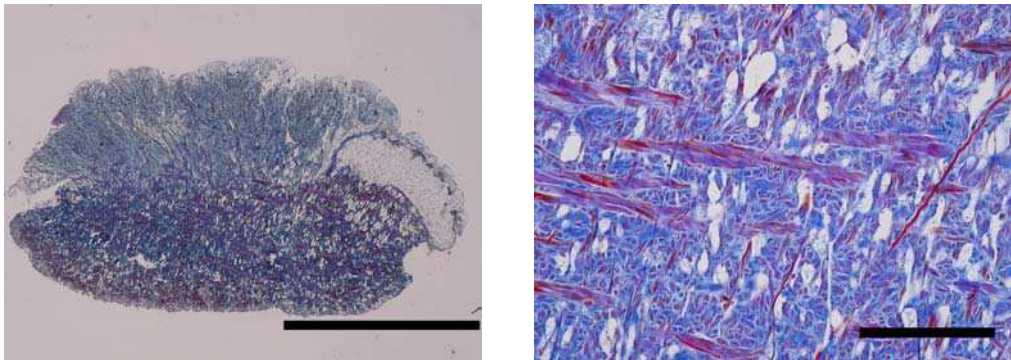


Fig. 1. The smooth muscle and connective tissue of gastropods. Mallory's blue trichrome, bar = 2 000 (left) and 200 (Right)  $\mu\text{m}$

##### *2.5.1. Volume Fractions of SMC and ECM*

Within the reference volume, equidistant sections were selected through systematic uniform random sampling (SURS). To estimate the relevant value of slides used for quantification  $m$ , i.e. the variation caused by sampling the serial sections, we used Gundersen and Jensen's method to predict the coefficient of error (CE) [5]. Preliminary pilot analysis proved that the number

of sections sampled within each tissue block had to be at least  $m = 12$  in order to keep the CE below 0.05. The position of the first tissue section in the volume was random, i.e. equal to  $(72 n/m)$ , where  $n$  was a random number between 0 and 1. Starting with that section, every sixth section was then captured.

We assessed the *volume fractions* of smooth muscle cells (SMC),  $V_V(SMC, ref)$ , and extracellular matrix (ECM),  $V_V(ECM, ref)$ , of the gastropod tissue using the point-grid test system placed on the micrograph of the tissue according to  $estV_V(component) = P_P(component)$ , where *component* was either SMC or ECM, and  $P_P(component)$  was the number of points  $P(component)$  of the test system lying on transections of SMC or ECM divided by total number  $P(total)$  of points of the test system [25]. The values of volume fractions of individual components were thus given by

$$estV_V(component) = P(component)/P(total) = P_P(component). \quad (1)$$

### 2.5.2. Length Density

The length density of SMC,  $L_V(SMC, ref)$ , was the mean total length  $L(SMC)$  of all fibres in an reference space divided by the volume of reference space  $V(ref)$ :

$$L_V(SMC, ref) = L(SMC)/V(ref). \quad (2)$$

In our case,  $L(SMC)$  was obtained using the line system approximating the centres of gravity of SMC.

### 2.5.3. Rose of Directions

The analysis of spatial systems of fibres is a frequent problem in biology, metallography and other applied sciences. Mathematically, these structures are often modeled as stationary fibre processes. The most basic characteristic is the length density  $L_V(fibres, ref)$  of fibres.

To describe anisotropy (preferential orientation) of the SMC, we used the stack of ten serial micrographs of the gastropod tissue. The micrographs were registered according to the  $z$ -axis and segmented with respect to the SMC using the software Imagreg1a (Jiří Janáček, Academy of Sciences of the Czech Republic, Prague, Czech Republic). The orientation of the stack w.r.t. the loading direction is sketched in fig. 2.

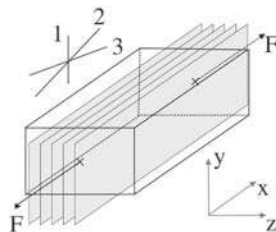


Fig. 2. Orientation of the stack of micrographs w.r.t. the loading direction. Indication of determined fibre directions (1, 2, 3)

The stack of registered micrographs was probed using the software Ellipse (module Tracer). The centres of gravity of all individual SMC in the stack were marked and approximated by lines, as illustrated in fig. 3. The resultant line system shown in fig. 4 was defined by the directions of individual lines and their lengths.

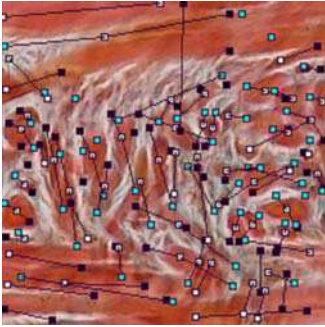


Fig. 3. One micrograph of the registered stack with lines (black) going through the centres of SMC. The points on current micrograph are colored white, on the previous micrograph are colored black and on the following micrograph are colored blue/gray

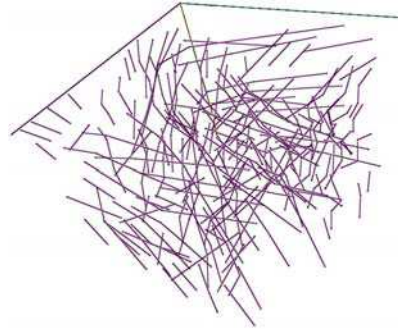


Fig. 4. The line system linking the centres of gravity of SMC. The coordinate system:  $x$ -axis (east-west),  $y$ -axis (north-east) and  $z$ -axis (north-south)

The half of the globe in  $\mathbb{R}^3$  was divided into various numbers of parallels and meridians. All divided tetragons had equal surface. Three intervals with the highest values of lengths of lines were selected and the azimuths and elevations were computed using Matlab (The MathWorks, Inc., Mattick, Massachusetts), giving thus the three preferential directions of fibres.

## 2.6. Mechanical Model of Gastropod Tissue

In [11] we have proposed a gastropod tissue model involving a hyperelastic and viscous matrix only. Here we improve the model by adding the fibres obeying the preferential directions determined in Section 3.1. The fibres should correspond both to muscle fibres in a passive state and collagen. To our knowledge, it is for the first time that a macroscopic gastropod tissue model is based on real tissue data and its parameters are identified from real measurements, see Section 3.2.

### 2.6.1. General Setting

The gastropod tissue exhibits large strains in both physiological conditions, as well as in our experiments. To model a body undergoing finite deformation, we employ the total Lagrangian (TL) formulation, cf. [20]. In this model all quantities and integrals are related to the initial (undeformed) configuration  $\Omega^{(0)}$  and the space derivatives are with respect to the material coordinates  $\underline{X}$ . The only unknown field are the displacements  $\underline{u}$ , but it is convenient to define also the pressure  $p$ , see below.

In the TL formulation the stresses in a body are characterized by the second Piola-Kirchhoff stress tensor  $\underline{S}$  which depends on the Green deformation tensor  $\underline{E} = \frac{1}{2}(\underline{C} - \underline{I})$ . Here  $\underline{I}$  is the identity tensor and  $\underline{C}$  is the right Cauchy-Green deformation tensor,  $\underline{C} = \underline{F}^T \underline{F}$ , where (using  $\underline{x} = \underline{X} + \underline{u}$ )  $\underline{F} = \frac{\partial \underline{x}}{\partial \underline{X}}$  is the deformation gradient. It is convenient to split  $\underline{S}$  into the effective (compression independent) part  $\underline{S}^{\text{eff}}$  and the volumetric (pressure) part  $-pJ\underline{C}^{-1}$ ,  $J = \det(\underline{F})$ , with  $p = -K(J - 1)$ . The near-incompressibility of living tissues, see e.g. [3], is treated by setting the bulk modulus  $K$  sufficiently large. Assuming the solution up to a step  $t$  to be known, we seek the solution at a step  $t + 1$  satisfying the equilibrium equation

$$\int_{\Omega^{(0)}} (\underline{\underline{S}}^{\text{eff}} - pJ\underline{\underline{C}}^{-1})^{(t+1)} : \delta \underline{\underline{E}}(\underline{v}) \, d\Omega - L^{(t+1)}(\underline{v}) = 0, \quad \forall \underline{v} \in V^3, \quad (3)$$

where  $L$  are the linear loads and  $V$  is a suitable function space. Note that in (3) we confine ourselves to a quasistatic problem solution.

### 2.6.2. Constitutive Relations

To define the constitutive relation for the effective (compression independent) part of the second Piola-Kirchhoff stress  $\underline{\underline{S}}^{\text{eff}}$  we employed our soft tissue model (cf. [17]) based on the theory of mixtures, where, in short, the total stress is a sum of volume fraction-weighted terms related to various components of the tissue. We have used a  $(n_f + 1)$ -component model consisting of the Mooney-Rivlin matrix and passive fibres in  $n_f$  preferential directions  $\underline{\underline{\nu}}^k$  (see Section 3.2:

$$\begin{aligned} \underline{\underline{S}}^{\text{eff}} = & \phi_m \left( \mu J^{-\frac{2}{3}} \left( \underline{\underline{I}} - \frac{1}{3} \text{tr}(\underline{\underline{C}}) - \frac{1}{3} \text{tr}(\underline{\underline{C}}) \underline{\underline{C}}^{-1} \right) + \kappa J^{-\frac{4}{3}} \left( \text{tr}(\underline{\underline{C}}) \underline{\underline{I}} - \underline{\underline{C}} - \frac{2}{3} I_2 \underline{\underline{C}}^{-1} \right) \right) \\ & + \sum_{k=1}^{n_f} \phi_p^k \tau^k(\varepsilon^k, \gamma_\infty^k, \bar{\varepsilon}_0^k, \beta^k, \gamma^k) \underline{\underline{\nu}}^k \underline{\underline{\nu}}^k, \end{aligned} \quad (4)$$

where  $\phi_m, \phi_p^k$  are volume fractions of the matrix and the passive fibres, respectively,  $\varepsilon^k = \underline{\underline{E}} : \underline{\underline{\nu}}^k \underline{\underline{\nu}}^k$  is the Green strain projected to the  $k$ -th fibre direction and  $\mu, \kappa, \gamma_\infty^k, \bar{\varepsilon}_0^k, \beta^k,$  and  $\gamma^k, k = 1, \dots, n_f,$  are constitutive parameters.

The fibres are described by the 3-parametric Kelvin model of viscoelasticity with a linear elastic response. Omitting the superscript  $k$ , the time-discretized viscoelastic tension is computed according to:

$$\tilde{\tau}^{(t+1)} = \frac{1}{c} \left[ \sigma(\underline{u}^{(t+1)}) + \gamma \left( \exp\{-\beta\Delta t\} h^{(t)} - \exp\{-\frac{\beta}{2}\Delta t\} \tau^{(t)} \right) \right], \quad (5)$$

$$\tau^{(t+1)} = \max\{0, \tilde{\tau}^{(t+1)}\}, \quad (6)$$

$$h^{(t+1)} = \exp\{-\beta\Delta t\} h^{(t)} + \exp\{-\frac{\beta}{2}\Delta t\} (\tau^{(t+1)} - \tau^{(t)}), \quad (7)$$

$$\tau^{(0)} = \sigma(\underline{u}^{(0)}), \quad (8)$$

$$h^{(0)} = 0, \quad (9)$$

where  $c = 1 - \gamma \exp\{-\frac{\beta}{2}\Delta t\}$  and  $\sigma(\underline{u}^{(t+1)}) = \gamma_\infty(\varepsilon^{(t+1)} - \bar{\varepsilon}_0)$  is the linear elastic response. The slack length  $\bar{\varepsilon}_0$  of a fibre can be used to prestress the fibre by setting it to a negative value. Note that due to (6) the fibres transmit a tension only, see fig. 5. For more details see [17].

### 2.7. Parameter Identification as Nonlinear Least Squares Problem

The method sketched below was originally developed in [18]. It was described in detail in [17] (general smooth muscle models) and applied to particular biomechanical models in [2] (kidney tissue), [19] (cardiac tissue), and [11] (pulmonate gastropod tissue).

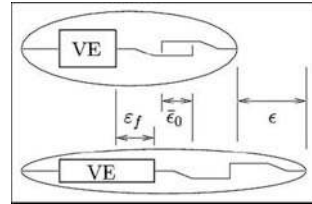


Fig. 5. Passive fibres: 3-parametric Kelvin model with tension-only property

The equilibrium equation (3) is discretized using the finite element method, and solved in a sequence of discrete time steps  $t = 0, \dots, T$ . Below, we call the discrete version of (3) a state problem, and denote it by  $\Phi^{(t)}(\alpha, y_t, y_{t-1}) = 0$ , to stress its dependence on the vector of (material) parameters to identify  $\alpha \in \mathbf{R}^n$ , and on the current and previous state vectors  $y_t, y_{t-1}$ . In our case  $y$  was simply a vector of displacements of the FE mesh nodes.

The task of identification of constitutive parameters of the gastropod tissue model (4) can be formulated in terms of the following nonlinear least-squares problem (NLS), seeking the vector  $\alpha_{aim} \in \mathbf{R}^n$  of the parameters:

$$\alpha_{aim} = \operatorname{argmin} \{F(\alpha) | \alpha = \{\alpha_i\}_{i=1}^n \in \mathbf{R}^n\}, \quad (10)$$

where the objective function  $F$  is given by

$$F(\alpha) \equiv \frac{1}{2} \sum_{i \in \mathcal{I}} (\varphi_i(\alpha, y_i) - \bar{\varphi}_i)^2. \quad (11)$$

The objective function measures a distance between the available measurements  $\bar{\varphi}_i$  and the simulated values of an observed quantity  $\varphi_i(\alpha, y_i)$ ,  $i \in \mathcal{I}$ , where  $\mathcal{I}$  is an index subset of the time steps with the measurements available. The state problem

$$\Phi^{(0)}(\alpha, y_0) = 0, \quad \Phi^{(t)}(\alpha, y_t, y_{t-1}) = 0, \quad t = 1, \dots, T \quad (12)$$

represents a principal constraint to the optimization method. Trivial (box) constraints  $\alpha_i^{\min} < \alpha_i < \alpha_i^{\max}$ , for some  $i$  can be added to make use of some apriori knowledge (thermodynamical considerations, biological limits, ...) of values of certain constitutive parameters.

### 2.7.1. Implementation Notes

The trust region interior-reflective Newton method (Matlab<sup>®</sup> implementation, see [14]) was used to perform the identification. This method works best when the gradients  $\nabla_{\alpha} F$  are provided, i.e. it is necessary to carry out the sensitivity analysis, cf. [17] or [11].

Because of the inevitable round-off errors in the computer finite precision arithmetic we avoid having very large and very small values of parameters together by scaling the parameters  $\alpha$  by a vector  $s$ . It is constructed out of the initial guess  $\alpha^0$  as follows:  $s_i = \alpha_i^0$  for  $|\alpha_i^0| > \epsilon$ ,  $s_i = 1$  otherwise, where  $\epsilon$  is a machine precision. Often the magnitudes of all the components of  $\alpha^0$  are greater than  $\epsilon$ , which leads to the scaled initial parameter vector of all ones.

The identification code can be used to estimate any combination of material parameters present in the constitutive relations. These parameters must be constant in time but they can be space dependent. The code enables to define *parameter clusters* — regions where a parameter is constant. Denoting the number of the clusters for the  $i$ th parameter by  $n_{\text{cluster}}^i$ , we have  $n = \sum_{i=1}^{n_{\text{par}}} n_{\text{cluster}}^i$ . A popular choice is to have only one cluster covering the whole mesh, which corresponds to a constant material parameter. In our applications these clusters are used, for example, to treat separately pathological regions, where some parameters (e.g. stiffness) may attain reduced values.

## 3. Results

### 3.1. Quantitative Microscopy

The relative volume proportion of SMC in tissue (without hemocoelic cavities) was estimated to be 58.9% and of ECM 41.1% according to the Cavalieri method.

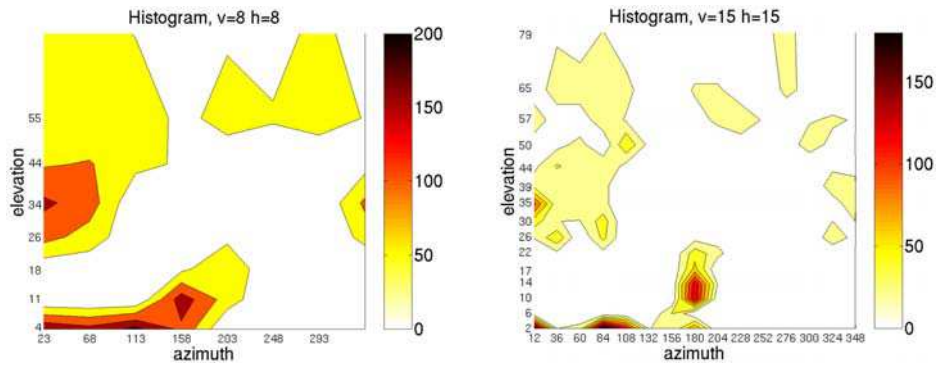


Fig. 6. Histograms of lengths of approximating lines for the number of parallels and meridians equal to eight (left) and fifteen (right)

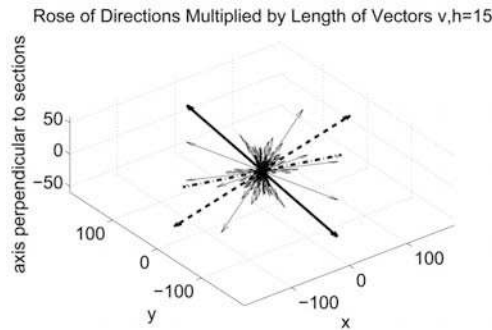


Fig. 7. The spatial rose of orientation of SMC of gastropod tissue for fifteen parallels and meridians

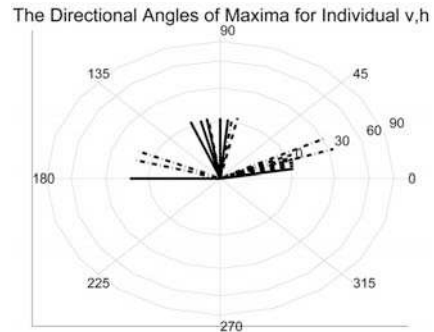


Fig. 8. The three preferential directions of SMC for various numbers of parallels and meridians; the descending histogram frequency order is: solid, dashed, dash-dotted line; azimuth: circumferential, elevation: radial

The total length of SMC in the stack was determined to be  $3\,171.1\ \mu\text{m}$ ; it was estimated using the line system approximating the centres of gravity of SMC. Using the total volume of the stack  $184\,774\ \mu\text{m}^3$  and (2) the length density of SMC was assessed to be  $0.0172\ \mu\text{m}^{-2}$ .

The total lengths of lines corresponding to given intervals of meridians and parallels are illustrated in fig. 6 and 7. The resultant three preferential directions of SMC in the gastropod tissue for various divisions of the spatial globe are shown in fig. 8. The Lambert azimuthal equal-area projection was used for the polar plots.

By examining the histograms, spatial roses and polar plots, we came to conclusion that the fibres lie preferably in the longitudinal-vertical ( $x$ - $y$ ) plane relative to the gastropod body; see fig. 8 (right), where all the elevation angles are close to zero. The highest histogram frequency was for fibres in the top-down ( $y$ ) direction and the second and third highest frequencies were for the longitudinal ( $x$ ) direction slightly tilted up and down, see also fig. 2, where the directions are indicated.

### 3.2. Parameter Identification

Below, we identify parameters of the model (4) using the same experimental data as in [11], where a simpler isotropic model without fibres was used. The consistent unit set {mm, s, kg: kPa, mN} will be used throughout this section, when not written explicitly.

### 3.2.1. Modelling assumptions and loading

According to the results of Section 3.1, the  $n_f = 3$  preferential directions of the fibres were used, see fig. 7, with  $\phi_p^k = 0.2$  for  $k = 1, 2, 3$  and thus  $\phi_m = 0.4$ . The direction vectors were chosen by examining the histograms, spatial roses and polar plots for varying number of parallels and meridians:  $\underline{\nu}^1 = [0, 1, 0]$ ,  $\underline{\nu}^2 = [0.9369, 0.3420, 0.0]$ ,  $\underline{\nu}^3 = [0.9369, -0.3420, 0.0]$ .

Two examples were considered: a creep test (T1) and a linear force test (T2). The tested specimens were assumed to be homogeneous, i.e. the material parameters were constants (one cluster over the entire mesh, and thus  $\alpha$  had 11 components:  $\alpha \equiv [\mu, \kappa, \gamma_\infty^1, \gamma^1, \beta^1, \gamma_\infty^2, \gamma^2, \beta^2, \gamma_\infty^3, \gamma^3, \beta^3]^T$ , as the slack lengths were set to 0. The bulk modulus was  $K = 1000$  kPa, high enough relative to the other elastic constants to provide a nearly incompressible material.

Due to the loading direction, the fibre system 1 was supposed to have no effect as it was under compression. We included it nevertheless, to verify this hypothesis.

### 3.2.2. Creep test

The experiment T1 lasted 1200 s with 3 s data acquisition step, while the simulation time step was 6 s. The physical dimensions of the specimen were  $5.33(x \text{ axis}) \times 2.43(y \text{ axis}) \times 3.9(z \text{ axis})$  mm. It was loaded by a constant stress of 10.6 kPa. The initial guess was

$$\alpha^0 = [10, 50, 125, 0.75, 1.25, 125, 0.75, 1.25, 125, 0.75, 1.25]^T.$$

After 22 NLS iterations taking 68 minutes the final parameters were

$$\alpha_{aim} = [2.18, 2.91, 125, 0.75, 1.25, 13.4, 0.891, 0.00056, 13.4, 0.891, 0.00043]^T,$$

see fig. 9, 10 and tab. 1.

*Discussion:* The initial parameters resulted in a rather stiff, elastic behaviour with almost no creep. In the course of the identification, the coefficients  $\beta^k$ ,  $k = 2, 3$  dropped by two orders to increase the creep time. Also the overall stiffness was significantly reduced ( $\mu, \kappa, \gamma_\infty^k$ ,  $k = 2, 3$ ). The  $k = 1$  fibres had no effect as expected.

Table 1. Summary of identification results for creep (T1) and linear force (T2) tests. Active box constraints are in bold.

$\alpha$	initial	final T1	final T2	$\alpha_i^{\min}$	$\alpha_i^{\max}$
$\mu$ [kPa]	10	2.18	0.102	0.001	1000
$\kappa$ [kPa]	50	2.91	68.5	0.001	1000
$\gamma_\infty^1$ [kPa]	125	125	125	0.001	1000
$\gamma^1$ [1]	0.75	0.75	0.75	0.1	0.95
$\beta^1$ [s <sup>-1</sup> ]	1.25	1.25	1.25	0.00001	2.5
$\gamma_\infty^2$ [kPa]	125	13.4	9.52	0.001	1000
$\gamma^2$ [1]	0.75	0.891	<b>0.1</b>	0.1	0.95
$\beta^2$ [s <sup>-1</sup> ]	1.25	0.00056	<b>2.50</b>	0.00001	2.5
$\gamma_\infty^3$ [kPa]	125	13.4	9.52	0.001	1000
$\gamma^3$ [1]	0.75	0.891	<b>0.1</b>	0.1	0.95
$\beta^3$ [s <sup>-1</sup> ]	1.25	0.00043	<b>2.50</b>	0.00001	2.5

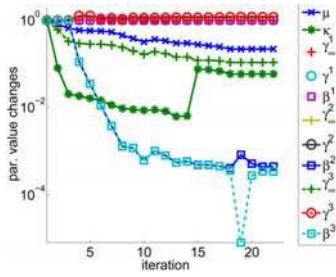


Fig. 9. Evolution of scaled parameters  $\bar{\alpha}$  (see Section 2.7.1) during NLS iterations, semilogarithmic scale of absolute values, creep test

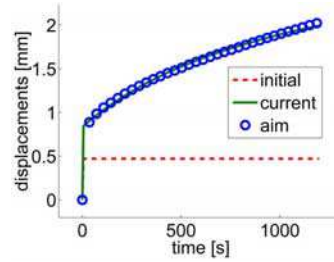


Fig. 10. Identification result, creep test: initial simulated observations (dashed line), final simulated observations (solid line) and experimental data (circles)

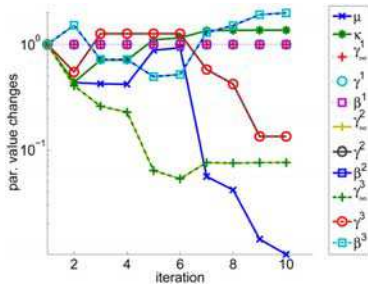


Fig. 11. Evolution of scaled parameters  $\bar{\alpha}$  (see Section 2.7.1) during NLS iterations, semilogarithmic scale of absolute values, linear force test

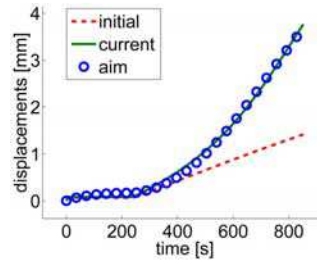


Fig. 12. Identification result, linear force test: initial simulated observations (dashed line), final simulated observations (solid line) and experimental data (circles)

### 3.2.3. Linear Force Test

In case T2, the experiment lasted 852 s with 6 s data acquisition step. The simulation time step was also 6 s. The physical dimensions of the specimen were 4.97(*x* axis) × 1.71(*y* axis) × 3.61(*z* axis) mm. It was loaded first by a constant pre-stress 1.6 kPa during 240 s and then the stress increased linearly by 3.24 kPa/minute (= force 20 mN/minute). The initial parameters  $\alpha^0$  were as in the test T1. After 10 NLS iterations taking 22 minutes the final parameters were

$$\alpha_{aim} = [0.102, 68.5, 125, 0.75, 1.25, 9.52, \mathbf{0.1}, \mathbf{2.50}, 9.52, \mathbf{0.1}, \mathbf{2.50}]^T,$$

see fig. 11, 12 and tab. 1.

*Discussion:* Here the results were completely different than in T1, besides the expected fact that  $k = 1$  fibres had no effect. The viscoelasticity of the  $k = 2, 3$  fibres was reduced as much as possible (both  $\gamma^k$  and  $\beta^k$  hit the box constraints, values marked bold) and the whole stress-strain curve was very well approximated by enlarging the Mooney-Rivlin coefficient  $\kappa$ . The response was thus almost purely hyperelastic.

### 3.2.4. Summary

The results of the two tests are collected in tab. 1. We may conclude that the measured displacements were well reproduced in both the cases. However, the same starting values resulted in

completely different identified parameters for the two cases. Possible causes, from the most to the least probable ones, can be

1. rather fast loading rate in T2 caused the elastic-like behaviour; the model of the fibres should be enhanced to capture this,
2. the sample for the quantitative microscopy represented a very small part of the gastropod foot; the preferential directions can vary within the sole, although visually the samples looked homogeneously,
3. physical samples were not exactly from the same part of the gastropod body for T1, T2.

#### 4. Conclusion

The volume fractions of smooth muscle cells (SMC) and extracellular matrix (ECM) in gastropod tissue were estimated. Moreover, the length density and spatial orientation of SMC, namely the rose of directions, and the three main directions of SMC were determined. These quantitative parameters of the gastropod smooth muscle and connective tissue were used in this extent for the first time, especially the rose of directions.

The model of gastropod tissue was presented, employing the determined volume fractions and the preferential directions. Its remaining constitutive parameters were identified using uniaxial loading tests by an automatic identification procedure based on nonlinear least squares. Very good fits were obtained for both the creep and linear force tests, although the model needs further attention to be able to encompass both those experiments at the same time.

The key contribution of the paper lies in a combination of quantitative microscopy, mechanical modeling and automatic parameter identification applied to one kind of soft tissue.

#### Acknowledgements

The work has been supported by the research project No. MŠM 4977751303.

#### References

- [1] M. Beranová and Z. Tonar. Principles and examples of immunohistochemistry [Principy a příklady imunohistochemie]. Grant FRVŠ F3 2082: Introduction of immunohistological methods into practical seminars of histology, Department of Histology and Embryology, Faculty of Medicine in Pilsen, Charles University, Prague, January 2002.
- [2] R. Cimrman, E. Rohan, and V. Nováček. Mechanical modelling and parameter identification of soft tissue: kidney case study. In *Proceedings of the 21 st conference Computational Mechanics 2005*, p. 111–118, Nečtiny, 2005.
- [3] Y. C. Fung. *Biomechanics. Mechanical Properties of Living Tissues*. Springer-Verlag, New York, second edition, 1993.
- [4] T. Ch. Gasser, R. W. Ogden, and G. A. Holzapfel. Hyperelastic modelling of arterial layers with distributed collagen fibre orientations. *Journal of the Royal Society Interface*, 3:15–35, 2006.
- [5] H. J. Gundersen and R. Osterby. Optimizing sampling efficiency of stereological studies: or ‘do more less well!’. *Journal of Microscopy*, 121:65–73, 1981.
- [6] H. J. G. Gundersen and E. B. Jensen. The efficiency of systematic sampling in stereology and its prediction. *Journal of Microscopy*, 147:229–263, 1987.
- [7] G. A. Holzapfel. Determination of material models for arterial walls from uniaxial extension tests and histological structure. *Journal of Theoretical Biology*, 238(2):290–302, 2006.

- [8] G. A. Holzapfel and T. C. Gasser. A viscoelastic model for fibre-reinforced composites at finite strains: Continuum basis, computational aspects and applications. *Computer Methods in Applied Mechanics and Engineering*, 190:4 379–4 403, 2001.
- [9] C. V. Howard and M. G. Reed. *Unbiased Stereology: Three Dimensional Measurement in Microscopy*. Microscopy Handbook Series No. 41. Royal Microscopical Society, Springer, New York, 1998.
- [10] M. Kiderlen. Non-parametric estimation of the directional distribution of stationary line and fibre processes. *Advances in Applied Probability*, 33:6–24, 2001.
- [11] P. Kochová, R. Cimrman, and E. Rohan. Parameter identification and mechanical modelling of smooth muscle and connective tissue. In *Proceeding of the conference Applied Mechanics*, p. 133–134, Malenovice, 2007.
- [12] P. Kochová and M. Holeček. Stress and stereological analysis of smooth muscle and connective tissue. In *Acta Mechanica Slovaca*, volume 1, p. 229–236, 2006.
- [13] P. Kochová and Z. Tonar. 3D reconstruction and mechanical properties of connective and smooth muscle tissue. In *Proceeding of the Conference Human Biomechanics 2006*, p. 120–121, Hrotovice, 2006. Brno University of Technology, Institute of Solid Mechanics, Mechanotronics and Biomechanics. Full version on CD-ROM.
- [14] MATLAB. *Optimization Toolbox, User's guide*. The Math Works Inc., 2005. Version 3.
- [15] P. R. Mouton, A. M. Gokhale, N. L. Ward, and M. J. West. Stereological length estimation using spherical probes. *Journal of Microscopy*, 206:54–64, 2002.
- [16] A. Nakano, M. Minamiyama, and J. Seki. The three-dimensional structure of vascular smooth muscle cells: A confocal laser microscopic study of rabbit mesenteric arterioles. *Asian Biomedicine*, 1(1):77–86, 2007.
- [17] E. Rohan and R. Cimrman. Sensitivity analysis and material identification for activated smooth muscle. *Computer Assisted Mechanics and Engineering Science*, 9:519–541, 2002.
- [18] E. Rohan and J. R. Whiteman. Shape optimization of elasto-plastic structures and continua. *Comput. Methods Appl. Mech. Engrg.*, 187:261–288, 2000.
- [19] J. Sainte-Marie, D. Chapelle, R. Cimrman, and M. Sorine. Modeling and estimation of the cardiac electromechanical activity. *Computers & Structures*, 84:1 743–1 759, 2006.
- [20] J. C. Simo and T. J. R. Hughes. *Computational Inelasticity*. Springer-Verlag, Berlin, 1998.
- [21] S. Standring. *Gray's Anatomy. The Anatomical Basis of Clinical Practice*. Elsevier Churchill Livingstone, Philadelphia, 2005.
- [22] D. Stoyan, W. S. Kendall, and J. Mecke. *Stochastic geometry and its applications 2nd ed.* John Wiley & Sons Ltd, New York, 1996.
- [23] Z. Tonar, P. Kochová, and J. Janáček. Orientation, anisotropy, clustering, and volume fraction of smooth muscle cells within the wall of porcine abdominal aorta. *Applied and Computational Mechanics*, 2(1):145–156, 2008.
- [24] Z. Tonar and A. Markoš. Microscopy and morphometry of integument of the foot of pulmonate gastropods *Arion rufus* and *Helix pomatia*. *Acta veterinaria Brno*, 73:3–8, 2004.
- [25] E. R. Weibel, G. S. Kistler, and W. F. Scherle. Practical stereological methods for morphometric cytology. *The Journal of Cell Biology*, 30:23–38, 1966.